Dynamic Poroelasticity Based Method for Falling Weight Deflectometer Test Analysis

Hongwei Liu, Pooneh Maghoul, & Ahmed Shalaby
University of Manitoba, Winnipeg, Manitoba, Canada

ABSTRACT
Pavement structures reach performance limits when there are multiple deteriorations caused by repeated vehicle loading and environmental effects. Therefore, acquiring detailed information about the state of the pavement structures is an important element in rehabilitation planning of sections showing significant damage. Falling Weight Deflectometer Test (FWD) is one of the most popular Non-Destructive Testing (NDT) techniques in characterization of the mechanical properties of the pavement structure. The FWD test measures the surface deflections caused by dropping a known mass from a specific height. Geophones are used to record the time histories of the vertical deflections of the pavement surface at various distances from the centre of the load-plate. The response at the surface calculated from Boussinesq theory (static analysis) and proposed dynamic analysis are compared. Furthermore, the damping effect of water on the FWD test data under dynamic load is investigated.

RÉSUMÉ
Les structures de la chaussée atteignent des limites de performance en cas de détériorations multiples causées par des charges de véhicules répétées et des effets environnementaux. Par conséquent, l'acquisition d'informations détaillées sur l'état des structures de la chaussée est un élément important de la planification de la réhabilitation des sections présentant des dommages importants. Le test du déflectomètre à masse tombante (FWD) est l'une des techniques de test non destructif (CND) les plus répandues dans la caractérisation des propriétés mécaniques de la structure de la chaussée. Le test FWD mesure les déformations de la surface causées par la chute d'une masse connue à une hauteur donnée. Les géophones enregistrent les historiques temporels des déviations verticales de la surface de la chaussée à différentes distances du centre du plateau de charge. La réponse à la surface calculée à partir de la théorie de Boussinesq (analyse statique) et de l'analyse dynamique proposée est comparée. De plus, l'effet de l'eau sur les données du test FWD sous charge dynamique est étudié.

1 INTRODUCTION

Non-destructive testing technique was developed in the mid-1950's for the pavement performance evaluation (Grau & Alexander, 1994). The Fall Weight Deflectometer (FWD) is one of the commonly used non-destructive techniques. FWD test measures the surface deflections induced by a dropping mass from a specific height onto a load plate placed on the pavement surface. Geophones are used to record the time histories of the vertical deflections of the pavement surface at various distances from the center of the load-plate. Several wave types will propagate through soil layers and reflect and diffract at layers' interfaces. Consequently, the reading obtained at the surface conveys information of the layers. These surface displacements are used later as the input of a back-calculation algorithm to determine the geological conditions and mechanical properties of the pavement layers.

The dynamic response analysis of saturated soil plays an important role in geotechnical engineering design, non-destructive testing and other geophysical applications. The falling weight deflectometer test is used to characterize the earth materials through the response measured at the surface. In this application, wave propagation in subgrades (porous medium) can be better represented using poroelasticity theory. The problem of dynamic poroelasticity has been solved through various methods. A direct boundary element approach for solving three-dimensional problems of dynamic poroelasticity in the time domain was developed by (Wiebe & Antes, 1991). The Boundary Element approach in the frequency domain was later presented by (Burridge & Vargas, 1979). The technique was based on an integral equation formulation in terms of solid displacements and fluid stress. The 2D and 3D fundamental solutions of dynamic poroelasticity was further developed by (Chen, 1994). The solutions were obtained in the Laplace transform domain and can be recovered to elastodynamics and steady state poroelasticity. In layered saturated media, similar approaches have been used by (Rajapakse & Senjuntichai, 1995) (Jianwen & Hongbing, 2004) . Other than boundary element method, finite element method has also been applied by (Panneton & Atalla, 1997). Finite difference method also used to simulate wave propagation in heterogeneous poroelastic media by (Wenzlau & Müller, 2009). In term of problem formulation, two options are commonly used in the literature, namely solid displacement versus pore-water pressure (u-p) and solid displacement versus relative fluid displacement (u-w).

The methods used to solve the dynamic poroelastic problem ultimately is used as a forward server. An optimization algorithm is required to further determine the dynamic soil properties given the measurement from the

surface. Various inverse algorithms have been developed and applied in the past 50 years. Full waveform inversion requires the numerical model and optimization algorithm to fit the measured waveform at the ground surface. (Beaty, Schmitt, & Sacchi, 2002) proposed Monte Carlo optimization (simulated annealing) to back-calculate the earth material properties by considering both fundamental and higher-mode Rayleigh wave dispersion curves. (Al-Khoury, Kasbergen, Scarpas, & Blaauwendraad, 2001) determined pavement properties of each layer using three algorithms: modified Levenberg–Marquardt, Powell hybrid and factored Secant update method. It is found that Powell is the most efficient algorithm for the inverse calculation. (Varma, Kutay, & Levenberg, 2013) presented a genetic algorithm to find the pavement material properties from FDW time history data.

In this paper, a analytical dynamic solution is developed for FWD test. The algorithm decoupled the field vector, displacement and porewater pressure, through Helmholtz decomposition in Laplace domain. The response at the surface due to a circular uniformly loading is compared using Boussinesq theory (static analysis) and proposed dynamic analysis. Furthermore, the damping effect of water on the vertical displacement and effective stress under dynamic load is investigated.

2 MODEL DESCRIPTION

2.1 Kinematic Assumptions

The linearized form of Green-Lagrange strain tensor, ε_{ij} for infinitesimal deforamtion is

$$\varepsilon_{ij} = \frac{1}{2}\left(u_{i,j} + u_{j,i}\right) \quad [1]$$

The skeleton's volume dilatation ε_{ij} is required to match the variations of connected pore spaces (or porosity) n because of the incompressibility of solid grains. Assumed constitutive rules are described next.

2.2 Constitutive Model

The constitutive law of the solid skeleton describing the stress-strain relations, is defined in terms of the effective stress $\sigma'_{ij} = \sigma_{ij} - \alpha p\delta_{ij}$, as

$$\sigma'_{ij} = \lambda\delta_{ij}\varepsilon_{kk} + 2\mu\varepsilon_{ij} - \alpha p\delta_{ij} \quad [2]$$

where σ'_{ij}, λ, μ, α, p are the effective stress, first Lame constant, second lame constant, Biot coefficient and the pore-water pressure respectively.

Meanwhile, the porewater pressure can be written as a function of displacement (u) and fluid displacement relative to soil skeleton (w):

$$\begin{aligned} p &= -\alpha M\varepsilon_{kk} + M\zeta \\ \zeta &+ w_{kk} = 0 \end{aligned} \quad [3]$$

where M is defined as $1/\left(\frac{n}{K_f} + \frac{\alpha - n}{K_s}\right)$ in which n is the porosity, K_f is the bulk modulus of fluid and K_s is the bulk modulus of the solid; ζ is the fluid content variation per unit volume.

2.3 Conservation Laws

The conservation law used to describe the motion of soil and fluid particles can be written as:

$$\begin{aligned} \sigma_{ji,j} + \rho\, g_i &= \rho\ddot{u}_i + \rho_f\ddot{w}_i \\ -P_{,i} + f &= \rho_f\ddot{u}_i + m\ddot{w}_i + b\dot{w}_i \end{aligned} \quad [4]$$

where g_i is the gravitational acceleration vector; ρ is the density of soil; ρ_f is the water density; m =$\rho_f\,\beta/n$ in which β is the tortuosity used to describe the diffusion properties in porous media; b = η/κ in which η is the viscosity of the fluid and κ is the permeability coefficient.

2.4 Governing Equations

Combining kinematic assumptions, constitutive models and conversations laws for solid skeleton and fluid particles, we can have:

$$\begin{aligned} \mu u_{i,jj} + (\lambda_c + \mu)u_{j,ji} + \alpha M w_{j,ji} &= -\rho\, g_i + \rho\ddot{u}_i + \rho_f\ddot{w}_i \\ \alpha M u_{j,ji} + M w_{j,ji} &= -\mathrm{f} + \rho_f\ddot{u}_i + m\ddot{w}_i + b\dot{w}_i \end{aligned} \quad [5]$$

where $\lambda_c = \lambda + \alpha^2 M$

The governing can be also written in frequency domain by performing convolution with $e^{-i\omega t}$. It should be mentioned that the governing equations in Laplace domain can be easily obtained by replacing ω with $i\,s$ (i^2 = -1 and s the Laplace variable).

3 ANALYTICAL SOLUTION USING U-P FORM

In order to obtain the analytical solution, Helmholtz decomposition is firstly used to decouple the fast P wave, slow P wave and s wave. The displacement vector usually is expressed as P wave scalar potential ϕ and shear wave vector $\vec{\psi}$. Since P wave exits in solid skeleton and fluid, two P wave potentials are used, ϕ_s and ϕ_f respectively.

$$\begin{aligned} \vec{u} &= \nabla\phi_s + \nabla\times\vec{\psi_s} \;\; and \;\; \nabla\cdot\vec{\psi_s} = 0 \\ \vec{w} &= \nabla\phi_f + \nabla\times\vec{\psi_f} \;\; and \;\; \nabla\cdot\vec{\psi_f} = 0 \end{aligned} \quad [6]$$

where ϕ is a scalar potential and ψ is a vector potential $(\psi_r, \psi_\theta, \psi_z)$.

Taking the divergence and curl of Equation 7 and using the vector identity $\nabla\cdot(\nabla\times\vec{u}) = 0$, $\nabla\times(\nabla\psi) = 0$, $-\nabla\times\left(\nabla\times(\nabla\times A)\right) = \nabla^2(\nabla\times A)$, Equation 7 can be decoupled into four wave equations as follows:

$$(\lambda_c + 2\mu)(\nabla^2\phi_s) + \alpha M\left(\nabla^2\phi_f\right) = -\rho\omega^2\phi_s - \rho_f\omega^2\phi_f$$

$$-\mu\left(\nabla^2\overrightarrow{\psi_s}\right) = \rho\omega^2\left(\overrightarrow{\psi_s}\right) + \rho_f\omega^2\left(\overrightarrow{\psi_f}\right)$$
$$\alpha M\left(\nabla^2\phi_f\right) + M\left(\nabla^2\phi_f\right) = -\omega^2\left(\rho_f\phi_f + \rho_m\phi_f\right) \qquad [7]$$

$$0 = \rho_f\omega^2\left(\overrightarrow{\psi_s}\right) + \rho_m\omega^2\left(\overrightarrow{\psi_f}\right)$$

The solution of dilation Wave (P waves) can be solved using Jordan norm form to decouple the wave equations involved with P wave. Similarly, the shear wave potentials can be solved by reducing PDE into two independent ODEs. By setting ψ_s as the component in θ direction and assume that the problem is axisymmetric, we can obtain the solution of above equations as shown in equation 8. The corresponding coefficients can be found in the Appendix.

$$\phi_s = p_{11}Ae^{-\sqrt{k^2+D_{11}}z}J_0(kr) + p_{12}Be^{-\sqrt{k^2+D_{22}}\,z}J_0(kr)$$

$$\phi_f = p_{21}Ae^{-\sqrt{k^2+D_{11}}\,z}J_0(kr) + p_{22}Be^{-\sqrt{k^2+D_{22}}z}J_0(kr) \qquad [8]$$

$$\psi_s = Ce^{-\sqrt{k^2+\frac{\left(\frac{\rho_f^2}{\rho_m}-\rho\right)\omega^2}{\mu}}z}J_1(kr)$$

3.1 Displacement, Stress and Pore-water Pressure

Consider a plain strain ($u_\theta = 0$) in an axi-symmetric condition $\left(\frac{\partial}{\partial\theta} = 0\right)$, the vector potential $\vec{\psi}$ has a component ψ_θ only. This property reduces the solution of the problem to following form:

$$u_r = \frac{\partial\phi_s}{\partial r} - \frac{\partial\psi_s}{\partial z}\ , \qquad u_z = \frac{\partial\phi_s}{\partial z} + \frac{1}{r}\frac{\partial(r\psi_s)}{\partial r}$$
$$\mathrm{w_r} = \frac{\partial\phi_\mathrm{f}}{\partial r} - \frac{\partial\psi_\mathrm{f}}{\partial z}, \qquad \mathrm{w}_z = \frac{\partial\phi_\mathrm{f}}{\partial z} + \frac{1}{r}\frac{\partial(r\psi_\mathrm{f})}{\partial r} \qquad [9]$$

The stress components and porewater pressure in cylindrical coordinate can be also written in terms of potentials:

$$\sigma_{zr} = \mu\left(\frac{\partial u_r}{\partial z} + \frac{\partial u_z}{\partial r}\right)$$

$$\sigma_{zz} = \lambda\left(\frac{\partial u_r}{\partial r} + \frac{u_r}{r} + \frac{\partial u_z}{\partial z}\right) + 2\mu\frac{\partial u_z}{\partial z} \qquad [10]$$

$$p = -\alpha M\left(\frac{\partial^2\phi_s}{\partial r^2} + \frac{1}{r}\frac{\partial\phi_s}{\partial r} + \frac{\partial^2\phi_s}{\partial z^2}\right) - M\left(\frac{\partial^2\phi_f}{\partial r^2} + \frac{1}{r}\frac{\partial\phi_f}{\partial r} + \frac{\partial^2\phi_f}{\partial z^2}\right)$$

3.2 Element with Infinite Depth

In geotechnical filed applications, the soil domain normally goes into infinite. Therefore, it is important to develop element with such feature to better represents the conditions in the reality. For this purpose, the 'one-node' element is developed to represent the infinite depth situation. When z is 0 (representing the top surface of a layer), above equation can be written as (in matrix form):

$$\begin{bmatrix} u_r \\ u_z \\ w_z \end{bmatrix} = \begin{bmatrix} -k\,P_{11} & -k\,P_{12} & k_s \\ -k_{p1}p_{11} & -k_{p2}p_{12} & k \\ -k_{p1}p_{21} & -k_{p2}p_{22} & -\frac{\rho_f}{\rho_m}k \end{bmatrix}\begin{bmatrix} A \\ B \\ C \end{bmatrix} \qquad [11]$$

Similarly, we can obtain the matrix for stress and pore-water pressure:

$$\begin{bmatrix} \sigma_{zr} \\ \rho_{zz} \\ p \end{bmatrix} = \begin{bmatrix} 2kk_{p1}p_{11}\,\mu & 2kk_{p2}p_{12}\mu & -(k^2+k_s^2)\mu \\ k_{p1}^2p_{11}(\lambda+2\mu) - k^2p_{11} & p_{12}\left(k_{p2}^2(\lambda+2\mu) - k^2\lambda\right) & -2kk_s \\ (k-k_{p1})(k+k_{p1})M(p_{11}\alpha+1) & (k-k_{p2})(k+k_{p2})M(p_{12}\alpha+1) & 0 \end{bmatrix}\begin{bmatrix} A \\ B \\ C \end{bmatrix}$$
[12]

4 LIMITING CASE: ELASTODYNAMICS

By setting α, ρ_f, m, b and M approaching zero, the following parameters can be reevaluated:

$$k_{11} \xrightarrow{\alpha=0,\rho_f=0,M=0} \frac{\omega^2\rho}{-2\mu-\lambda}$$
$$k_{12}\,, k_{21}, k_{22} \xrightarrow{\alpha=0,\rho_f=0,M=0} 0 \qquad [13]$$

Similarly, the value of D_{11} goes to $\frac{\omega^2\rho}{-2\mu-\lambda}$ and D_{11} goes to zero when poroelastic paraemters approachs to zero. Then the solution of the potentials ϕ_s and ψ_s is identical to the elastic case. The term ϕ_f and ψ_f will eventually dispear with soil is in dry case.

5 CASE STUDY

5.1 Surface Load Description

In this section, the response of pavement subgrade under FWD test is studied. A schematic plot of FDW on subgrade is shown in Figure 1. A uniformly distributed normal force is applied on a circular plate with a radius of 0.15m at the surface. The applied pressure on the loading plate is a function o time and it follows the distribution (Gaussian function) shown in Figure 2. The spatial distribution of such load can be seen in Figure 3. The spatial load representation is enhanced using Ceasaro summation. The idea is that the weight of Fourier-Bessel series is multiplied by $\frac{\mathrm{n}+1-\mathrm{m}}{\mathrm{n}+1}$, in which n is the total mode number.

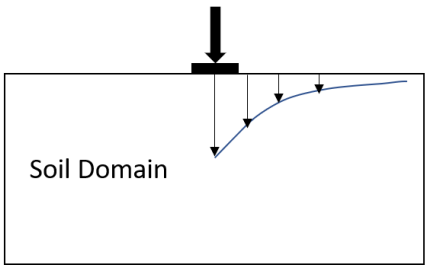

Figure 1 Schematic plot of Falling Weight Deflectometer test

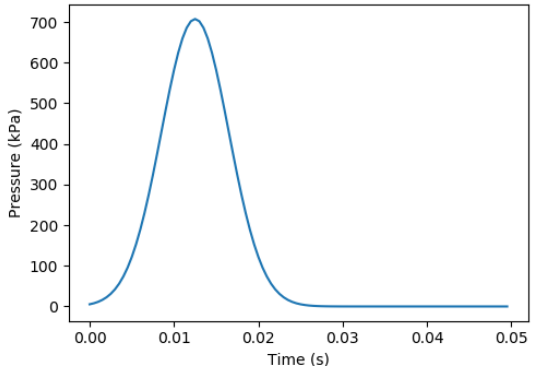

Figure 2 Applied pressure distribution with time at surface.

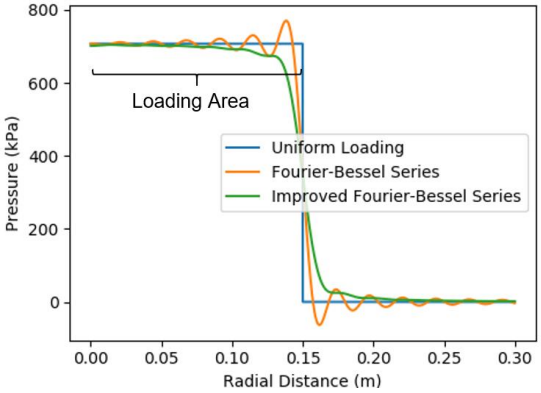

Figure 3 Spatial load distribution using classical vs improved Fourier-Bessel series method

5.2 Comparison with Boussinesq Theory

According to Boussinesq theory, the vertical elastic settlement at the surface due to a circular uniformly loaded area can be calculated as:

$$\Delta z = \frac{q_s D (1-\mu^2)}{E}$$

where q_s is the loading pressure, as shown in Figure 2; D is the loading area diameter, taken as 0.3m. The value of E and μ is 100MPa and 0.33, respectively.

A comparison between displacement calculated from Boussinesq theory and current algorithm can be seen in Figure 4. In Boussinesq method, the soil displacement at current time step is independent to that at previous step, which is not the case in proposed dynamic method. It is concluded that the results in terms of displacement from Boussinesq methods and proposed methods showed the agreement to some extent in single layer system.

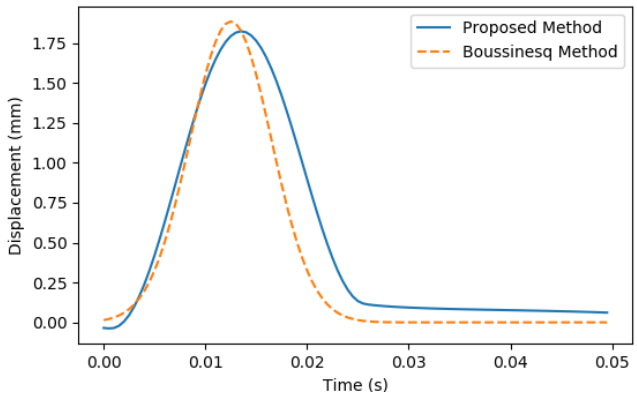

Figure 4 Vertical displacement increment comparison using proposed and Boussinesq method

Similarly, the induced vertical stress is also compared. Based on Boussinesq theory, the increases of vertical stress under the center of loading area is expressed as:

$$\Delta\sigma_z = q_s \left[1 - \left(\frac{1}{1 + (r_o/z)^2}\right)^{3/2}\right]$$

The vertical stress increment at 1m depth is shown in Figure 5. In static analysis (Boussinesq theory), only compression exits, and its value is linearly dependent on the external load. In dynamic analysis using the proposed method, both compression and tension are applied to the soil.

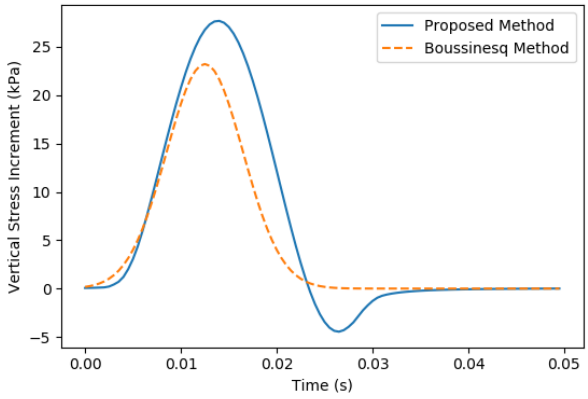

Figure 5 Vertical stress increment comparison using proposed and Boussinesq method at a 1m depth.

In multilayer system, the wave interactions become important. The results from those two methods will be very different, especially with bedrock located in shallow depth. In this case, the Young's modulus and Poisson ratio is taken as the average value of first three layers for Boussinesq methods. The values used in this analysis is shown in Table 1.

Table 1. Characteristics of pavement material properties

Method	Layer	E (MPa)	μ	$\rho\ (kg/m^3)$	H(m)
Proposed method	1st layer	1000	0.35	2300	0.15
	2nd layer	500	0.35	1800	0.25
	3rd layer	100	0.35	1500	2.6
	Bedrock	2000	0.2	2500	∞
Boussinesq	-	533	0.35	-	-

The vertical displacement at surface suing proposed method and Boussinesq method can be seen in Figure 6. With elastic bedrock located below subgrades, the stress wave induced by the impact load can be reflected immediately, which can be visualized as fluctuation of displacement at the surface. Such phenomena can't be captured by static analysis.

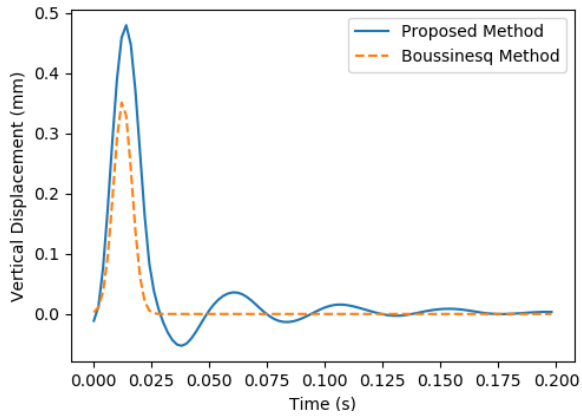

Figure 6 Vertical displacement increment with bedrock located at 3m depth using proposed and Boussinesq method

6 DAMPING EFFECT OF WATER

6.1 One Layer System

In this section, the effect of water content on the response of subgrade (including displacement, effective stress and porewater pressure) is studied. It is assumed that the drained condition is applied at the surface of the semi-infinite porous subgrade. The soil parameters used for dynamic poroelastic analysis is shown in table 2.

Table 2. Characteristics of subgrades soils

Properties	Value
Poisson ratio (μ)	0.35
Viscosity (η)	$10^3\ (Pa \cdot s)$
Permeability (κ)	$10^{-9}(m/s)$
Water density (ρ_f)	1000 (kg/m^3)
Bulk density (ρ)	1800 (kg/m^3)
Tortuosity (β)	0.9
Fluid bulk modulus (K_f)	2000 (MPa)
Youngs' modulus (E)	100 (MPa)

The vertical displacement at the surface under dry and fully saturated conditions (with porosity of 0.2 and 0.8) are shown in Figure 7. The response under dry condition is calculated using dynamic elasticity. It shows that when soil is fully saturated, the induced vertical displacement is reduced in comparison with soil under dry conditions with no porosity. With higher porosity, the available path for stress wave in solid skeleton is reduced, which essentially decrease the overall stress wave travelling speed. Such phenomena are considered as damping effect and eventually the vertical displacement measurement at the surface is reduced.

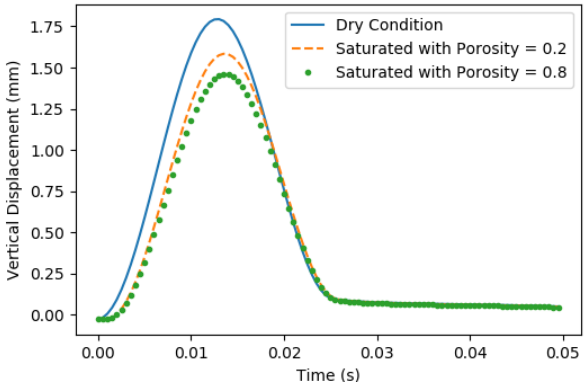

Figure 7 Vertical displacement increment at surface under dry and saturated conditions

The effective stress and porewater pressure for saturated soil with porosity of 0.2 is shown in Figure 8. The induced effective stress at 1m depth is also reduced in comparison with that under dry condition (shown in Figure 5) due to the damping effect of water.

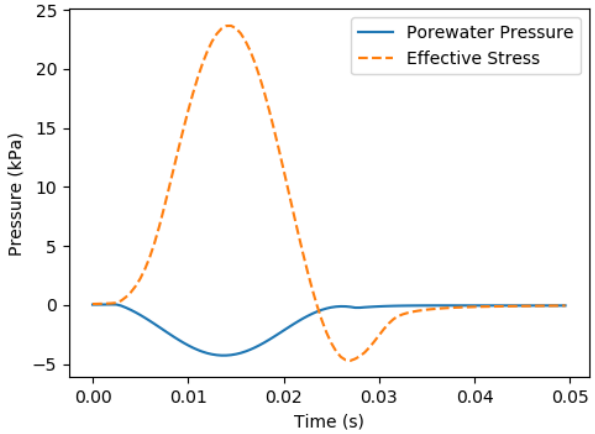

Figure 8 Porewater pressure and effective stress variation at 1m depth in fully saturated situation

6.2 Multilayer Layer System

In this case study, a three-layer system consisting of asphalt, subbase and subgrade are studied. The vertical displacement distributions are compared when subgrade is dry (no porosity) and fully saturated with porosity of 0.5. The parameter can be found in Table 1 and Table 2 under dry and saturated case. The sensors (geophones) are assumed to be placed at the center of loading plate, and 0.6m away from the center. The induced displacement in both cases can be seen in Figure 9. It shows that porewater provides damping effect under repaid dynamic loadings.

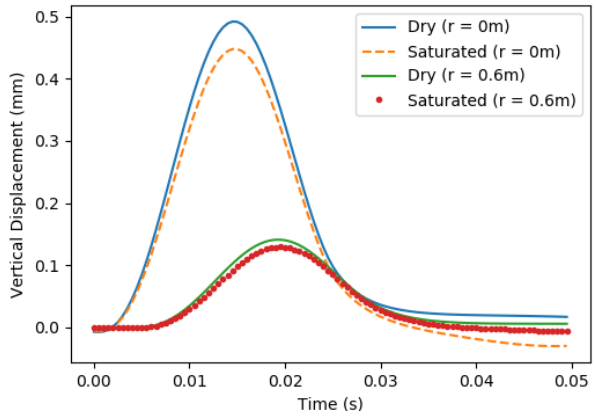

Figure 9 Induced displacement measured at center and 0.6m away at the surface for dry and saturated case

7 CONCLUSION

In this paper, a 3D semi-analytical solution was obtained to study the dynamic response of pavement under FWD loading test. It is concluded that in single layer system, static analysis based on Boussinesq theory can roughly predict the vertical displacement. However, in multilayer system where stress wave reflective becomes important, dynamic analysis are required. Based on the proposed model, it is found that the existence of porewater decreases the overall stress wave travelling speed. Consequentially, the induced displacement and effective stress are reduced due to the damping effect of water.

8 ACKNOWLEDGMENT

This research was partially supported by University Research Grants Program (2018) and Strat-Up Fund (2015-2018), University of Manitoba. The authors would like to acknowledge the software platform provided by COMSOL Inc. and CMC Microsystems.

9 REFERENCES

Abate, J., & Valkó, P. P. (2004). Multi-precision Laplace transform inversion. *International Journal for Numerical Methods in Engineering, 60*, 979-993.

Al-Khoury, R., Kasbergen, C., Scarpas, A., & Blaauwendraad, J. (2001). Spectral element technique for efficient parameter identification of layered media: Part II: Inverse calculation. *International Journal of Solids and Structures, 38*, 8753-8772.

Ahsan, M., and Choudhry, M.A. 2017. System identification of an airship using trust region reflective least squares algorithm. International Journal of Control, Automation and Systems, **15**(3): 1384–1393. doi:10.1007/s12555-015-0409-0.

Beaty, K. S., Schmitt, D. R., & Sacchi, M. (2002). Simulated annealing inversion of multimode Rayleigh wave dispersion curves for geological structure. *Geophysical Journal International, 151*, 622-631.

Burridge, R., & Vargas, C. A. (1979). The fundamental solution in dynamic poroelasticity. *Geophysical journal international, 58*, 61-90.

Chen, J. (1994). Time domain fundamental solution to biot's complete equations of dynamic poroelasticity Part II: three-dimensional solution. *International Journal of Solids and Structures, 31*, 169-202.

Grau, R. H., & Alexander, D. R. (1994). *Nondestructive Testing, Evaluation, and Rehabilitation for Roadway Pavement: Warren County, Mississippi, Cincinnati, Ohio, and Berkeley, California.* Tech. rep., ARMY ENGINEER INST FOR WATER RESOURCES FORT BELVOIR VA.

Jianwen, L., & Hongbing, Y. (2004). Dynamic stiffness matrix of a poroelastic multi-layered site and its Green's functions. *Earthquake Engineering and Engineering Vibration, 3*, 273.

Zhang, P., and Geers, T.L. 2005. Excitation of a fluid-filled, submerged spherical shell by a transient acoustic wave. The Journal of the Acoustical Society of America, **93**(2): 696–705. doi:10.1121/1.405433.

APPENDIX

$$k_{11} = \frac{\omega^2(\rho-\alpha\rho_f)}{M\alpha^2-2\mu-\lambda_c};\ k_{12} = \frac{\omega^2(\rho_f-\alpha\rho_m)}{M\alpha^2-2\mu-\lambda_c},$$

$$k_{21} = \frac{\omega^2\left((2\mu+\lambda_c)\rho_f-M\alpha\rho\right)}{M(M\alpha^2-2\mu-\lambda_c)} \text{ and } k_{22} = \frac{\omega^2\left((2\mu+\lambda_c)\rho_m-M\alpha\rho_f\right)}{M(M\alpha^2-2\mu-\lambda_c)}$$

$$D_{11} = \frac{1}{2}\left(-\sqrt{(k_{11}-k_{22})^2+4k_{12}k_{21}}+k_{11}+k_{22}\right),$$

$$D_{22} = \frac{1}{2}\left(\sqrt{(k_{11}-k_{22})^2+4k_{12}k_{21}}+k_{11}+k_{22}\right),$$

$$\mathrm{P}_{11} = -\frac{\sqrt{(k_{11}-k_{22})^2+4k_{12}k_{21}}-k_{11}+k_{22}}{2k_{21}},$$

$$\mathrm{P}_{12} = \frac{\sqrt{(k_{11}-k_{22})^2+4k_{12}k_{21}}+k_{11}-k_{22}}{2k_{21}}.$$